Supporting Information

Designing interconnected passages by "legs-to-head" directional U-shape freeze casting to boost solar-driven self-pumping oil spill recovery

Shiwen Wu[1], Amirarsalan Mashhadian[1], Ruda Jian[1], Siyu Tian[1], Tengfei Luo[2], Guoping Xiong[1,*]

[1.] Department of Mechanical Engineering, The University of Texas at Dallas, Richardson, Texas 75080, USA

[2.] Department of Aerospace and Mechanical Engineering, University of Notre Dame, Notre Dame, Indiana 46556, USA

* Corresponding author: Guoping Xiong: guoping.xiong@utdallas.edu

Section S1 Experimental Methods

S1.1 Preparation of GO

GO was synthesized following our prior work[1,2]. Typically, 2.4 g of expandable graphite flakes (>50 mesh, Sigma-Aldrich) were thermally expanded in a microwave oven (900W, Danby) for 30 s. The expanded graphite flakes were transferred into a mixture consisting of 224 mL of concentrated H_2SO_4 (95-98%, Sigma-Aldrich) and 16 mL of concentrated H_3PO_4 ($\geq$ 85%, Sigma-Aldrich) and kept in an ice bath. After slowly adding 8 g of $KMnO_4$ ($\geq$ 99%, Sigma-Aldrich) into the mixture within 2 h, the solution was transferred to a 50℃ water bath and further stirred for 5 h. Finally, 200 mL of iced deionized (DI) water was added into the solution, followed by dropwise adding H_2O_2 (30 wt.%, Sigma-Aldrich) until the solution became bright yellow. The as-obtained solution was repeatedly centrifuged with 1 M HCl solution (diluted from 37% HCl solution, Sigma-Aldrich) and sequentially DI water until the supernatant is neutral. The as-obtained GO paste was freeze-dried for 48 h to obtain GO powder.

S1.2 Fabrication of the Oil Skimmers

U-shape WOSs at various angles were prepared through a directional "legs-to-head" freeze-casting process. In a typical procedure, GO powder was dispersed in DI water using sonication to obtain GO aqueous suspensions (10 mg/mL). Then, GO suspension was poured into a 3D-printed U-shaped mold. Two copper strips were employed, with one end immersed in liquid nitrogen, and the other attached to the end of the "legs" of the mold. After completely freezing the suspension, the GO/ice block was demolded and freeze-dried for 48 h in a lyophilizer (BK-FD10S, Biobase). The as-obtained structure was subsequently annealed at 800℃ for 2 h under argon atmosphere in a tube furnace (DSP-1200-KS, TMAX) to obtain the 3D graphene

monoliths. Graphene petals (GPs) were grown on the surface of the graphene monolith through a customized inductively coupled plasma enhanced chemical vapor deposition (PECVD) system. In a typical procedure, 3D graphene monoliths were placed in a sealed cylindrical quartz tube, vacuumed to <10 Pa, and heated to 800 °C. A gas flow of CH_4 (6 mL min^{-1}) and H_2 (6 mL min^{-1}) was then injected into sealed tubes to act as precursors of GPs, with the growth pressure maintained at ~40 Pa. Subsequently, a radio frequency source of 300 W was coupled into the quartz tube. After growth for 2 h, the sample was cooled down under the protection of 20 mL min^{-1} Ar flow to obtain the WOS samples. For comparison, ROSs were fabricated following the same procedures but directly frozen in a cold environment (approx. -150°C).

Oil skimmers fabricated by ambient drying process were also employed as the control groups. Briefly, mixtures of camphene (20 mL) and GO solutions (20 mL, 20 mg/mL) were heated in a water bath kept at 70°C. Then, sodium dodecyl sulfate solutions (0.5 mL, 250 mg/mL) were added to the mixtures, followed by mechanical shaking to form homogeneous GO/camphene emulsions with the same concentration of GO, 10 mg/ml, compared to ROSs and WOSs. The GO/camphene emulsions were cast into the 3D-printed U-shaped molds and dried under ambient conditions (25°C, 1 atm, 50% RH) to obtain GO aerogels. The as-obtained structures were subsequently annealed at 800°C for 2 h under argon atmosphere in a tube furnace to obtain the ambient-dried oil skimmers.

S1.3 Materials Characterization

Scanning electron microscope (Sigma 500VP, Zeiss) was applied to characterize the morphology of the samples. An ultraviolet–visible–near-infrared spectrophotometer (Cary UV-Vis-NIR models 7000) with external diffuse reflectance accessories (DRA) 150 mm

integrating sphere was used to measure the photonic transmittance (T) and reflectance (R). Photonic absorbance (A) was calculated by $A = 1 - T - R$.

S1.4 Oil Recovery Tests

The oil recovery tests were conducted under a solar simulator (94023A, Newport Corporation, 450 W Xenon light source) with a <3° collimated output. An air mass 1.5G filter was employed to modify the spectral output to match the solar spectrum. Before the tests, the solar simulator was adjusted to obtain desired intensities through an optical power meter (S401C, Thorlabs). An infrared camera (A655sc, FLIR) was used to characterize the surface temperature distribution of the samples. An electronic balance (AS120.R2, Radwag) was employed to record the mass of collected oil every 30 seconds. All the experiments were conducted in a windless environment with a room temperature of ~ 23°C and relative humidity of ~ 49%. Error analyses were conducted based on multiple sets of repeatable tests.

Section S2 Supplementary Figures

The concentration of GO solutions significantly affects the microstructure, wettability, and oil recovery performance of WOS-60s. WOS-60s fabricated with solutions containing GO concentrations of 5 and 10 mg/mL display well-aligned channels in the "leg" parts. The channels are wider in skimmers fabricated with solutions containing 5 mg/mL GO compared to those in samples prepared with 10 mg/mL GO solutions. At a higher GO concentration of 20 mg/mL, the channels become distorted and less aligned along the freezing direction. Moreover, the water contact angle on WOS-60s increases with the GO concentration, which can be attributed to the different pore structure of these samples. The oil recovery rate improves as the GO concentration decreases, resulting from the reduced flow resistance from well-aligned channels with large widths at lower concentrations. We note that while high oil recovery rates are achievable at low GO concentrations, the mechanical properties of the skimmers deteriorate, as demonstrated in our prior work[3].

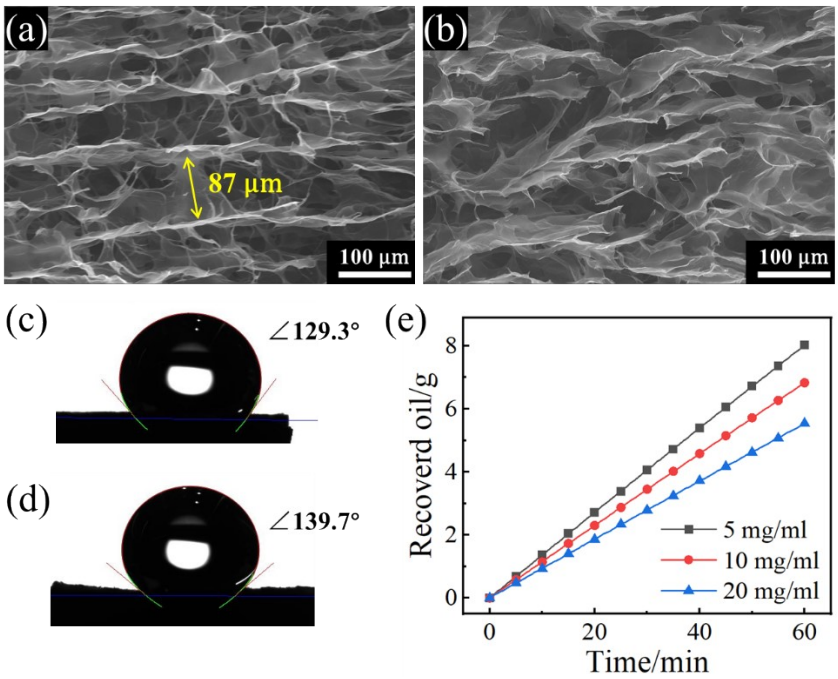

Figure S1. SEM images depicting the cross-sectional morphology of the "legs" for WOS-60 fabricated with (a) 5 mg/mL and (b) 20 mg/mL GO solutions. Water contact angle on WOS-60 fabricated with (c) 5 mg/mL and (d) 20 mg/mL GO solutions. (e) Mass evolution of oil collected under dark conditions by WOS-60 fabricated with different GO concentrations.

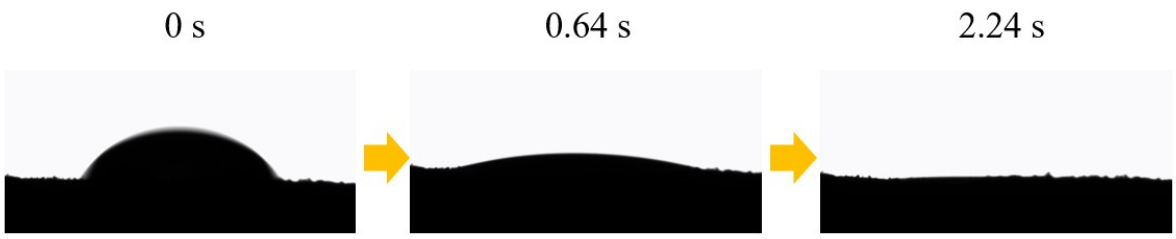

Figure S2. Contact angle of oil droplet on WOS-60.

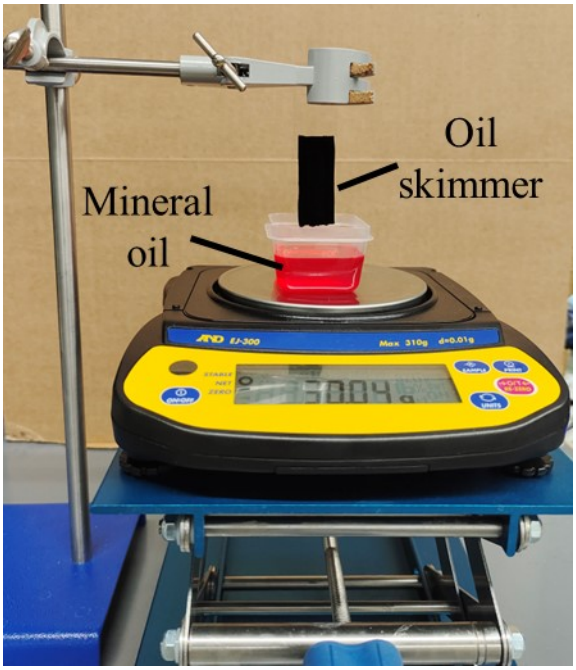

Figure S3. Photograph showing the home-made oil wicking test setup.

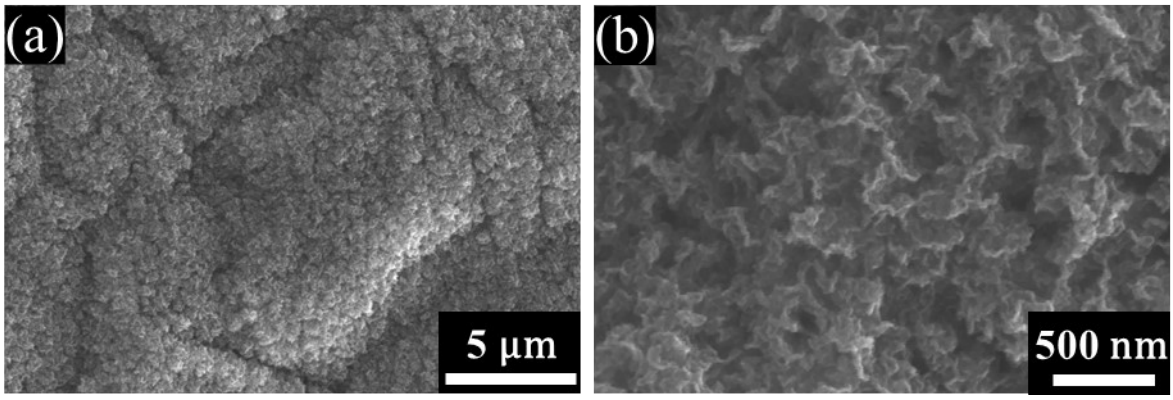

Figure S4. SEM images of GPs grown on the surface of WOS-60.

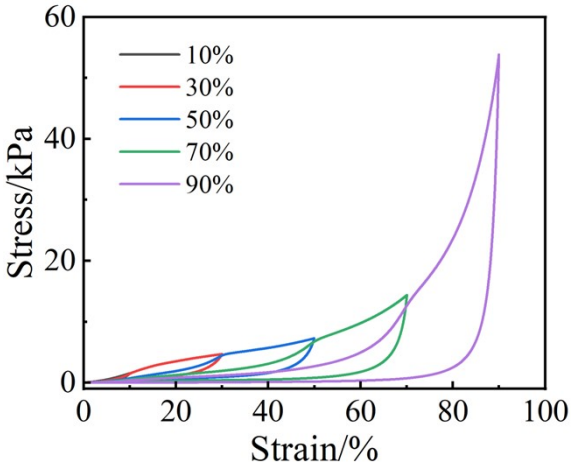

Figure S5. Stress-strain curves of WOSs at different compressive strains. The density of WOSs is measured to be 4.1 mg cm^{-3}.

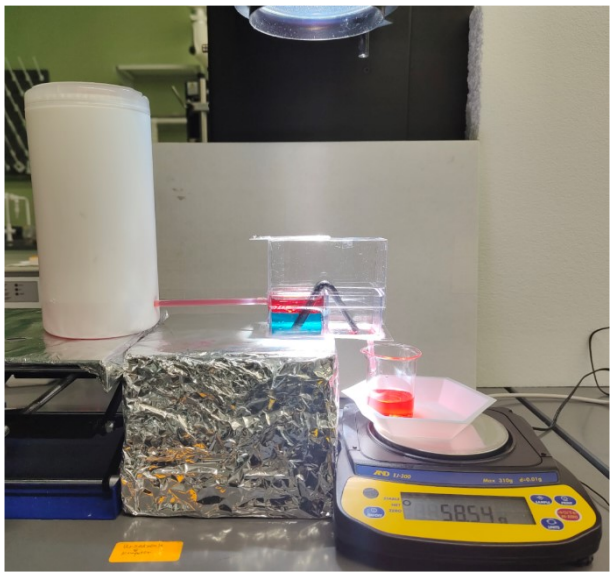

Figure S6. Photograph showing the lab-scale oil recovery test setup.

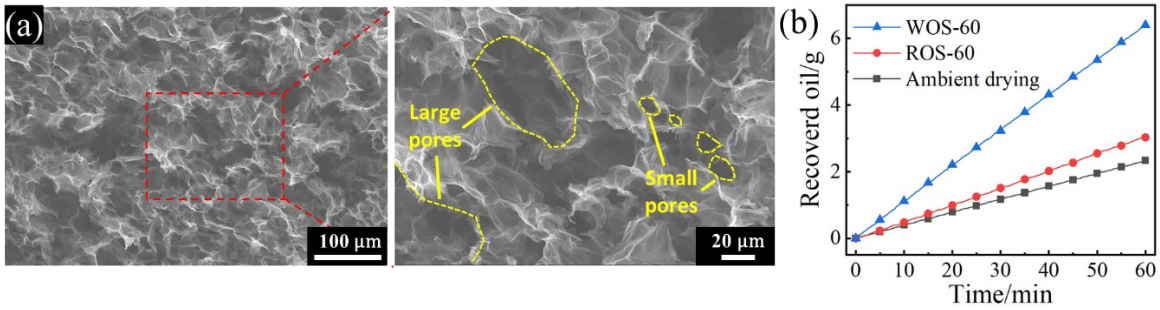

Figure S7. (a) SEM images depicting the cross-sectional morphology of ambient-dried oil skimmers. (b) Mass evolution of oil collected by WOS-60, ROS-60, and the ambient-dried oil skimmers under dark conditions.

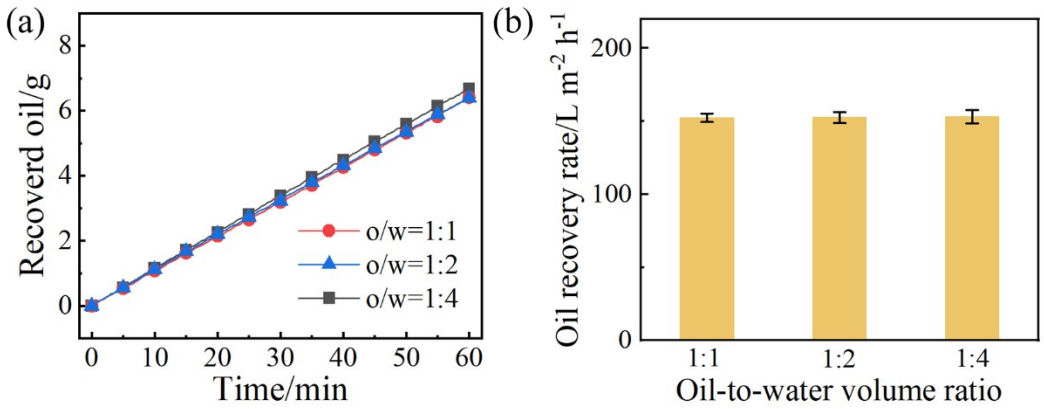

Figure S8. (a) Mass evolution of oil collected by WOS-60 under dark conditions with different oil-to-water volume ratios (o/w). (b) Calculated oil recovery rates of the WOS-60 under dark conditions with different oil-to-water volume ratios.

2 mL different oil samples are placed on a hot plate surface kept at 120℃ for 1 h to completely remove contained water. Mass change of pure oil (Δm) is also measured for comparison. The water content (C) in the oil samples can thus be calculated as:

$$C = \frac{m_1 - m_2 - \Delta m}{m_1} \times 100\% \qquad (S1)$$

where m_1 and m_2 are the mass of oil samples before and after heating, respectively. The measured data are shown in Figure S6. The separation efficiency (η_s) of the WOS-60 is determined by the water content before (C_b) and after (C_a) oil recovery[2,4,5]:

$$\eta_s = \left(1 - \frac{C_a}{C_b}\right) \times 100\% \qquad (S2)$$

As a result, the separation efficiencies of oil recovery from oil/water mixture by fresh WOS-60 and WOS-60 stored for 2 months are calculated to be 99.92% and 99.85%, respectively.

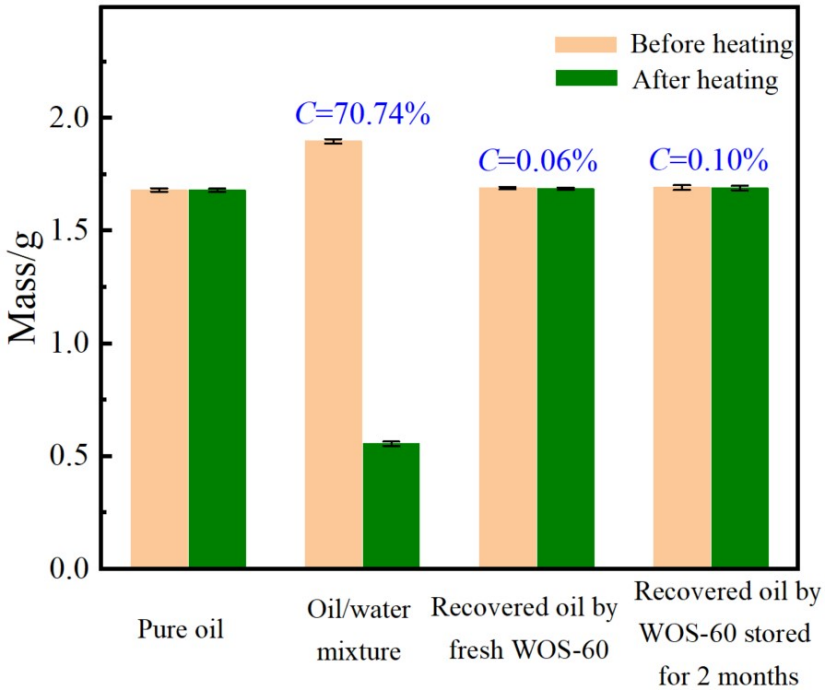

Figure S9. Recorded mass of different oil samples (2 mL) before and after heating at 120℃ for 1 h. Corresponding water contents of different oil samples are calculated based on Equation S1.

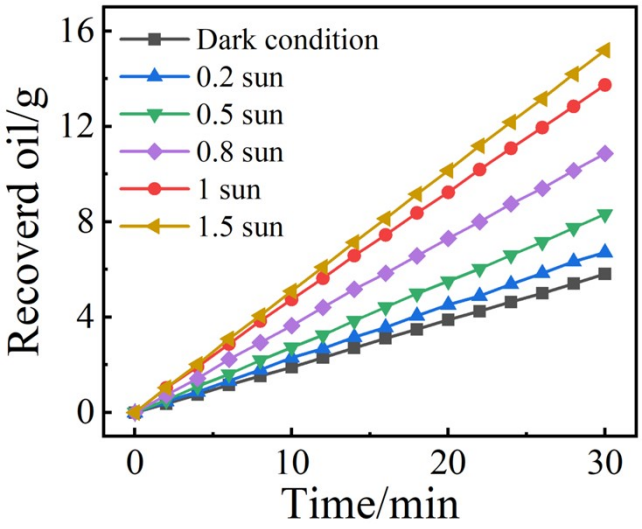

Figure S10. Mass evolution of recovered oil by the WOS-60 working under different solar intensities.

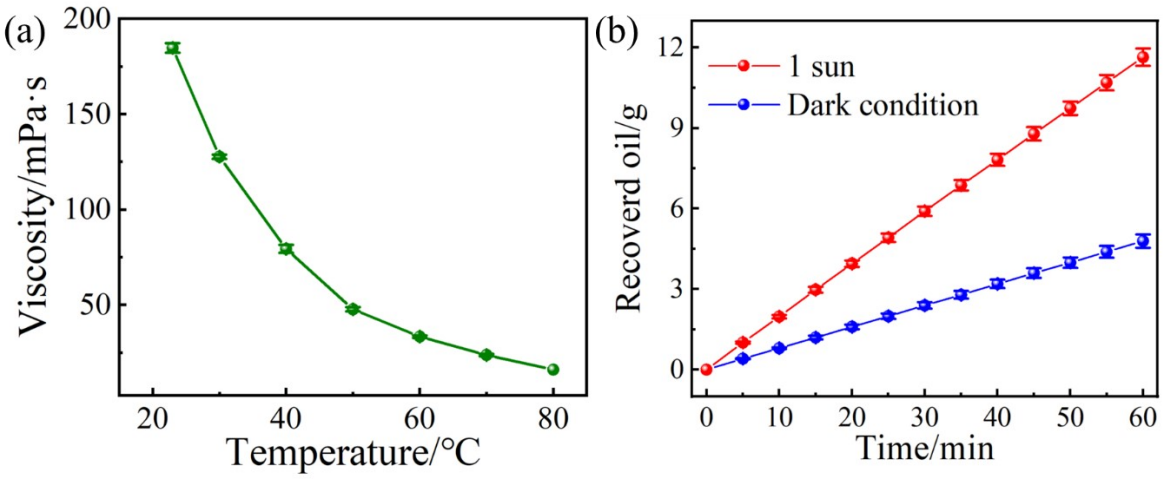

Figure S11. (a) Viscosity of oil-II as a function of temperature. (b) Mass evolution of recovered oil-II by the WOS-60 at 1 sun and under dark condition at ΔH of 55 mm.

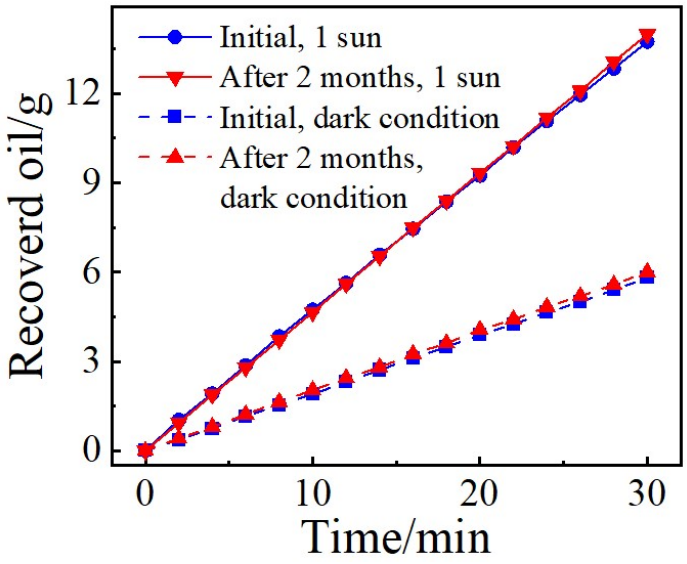

Figure S12. Comparative mass evolution of recovered oil by the fresh WOS-60 and WOS-60 stored for two months under 1 sun of solar irradiation and dark condition.

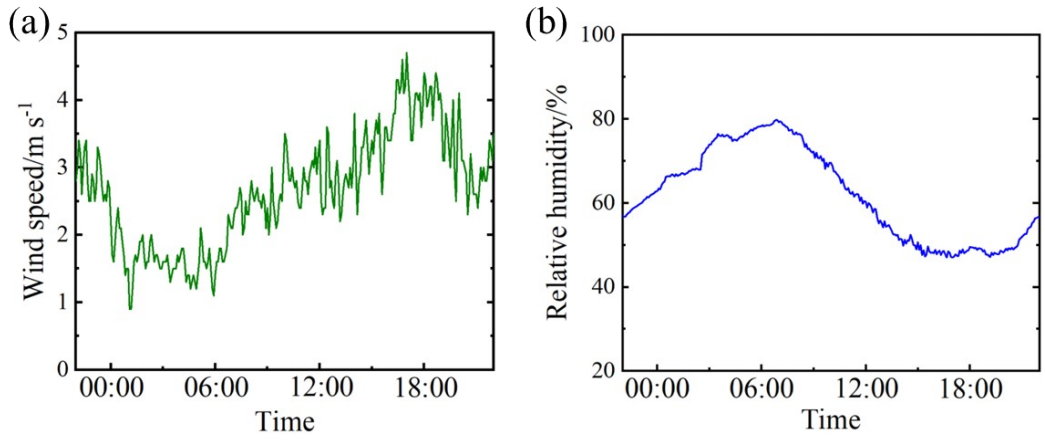

Figure S13. (a) Wind speed and (b) Relative humidity over time during the outdoor test.

Table S1. Comparison of oil recovery performance between the WOSs and previous oil recovery devices

Year/Journal	Type of oil recovery device	Oil type	Oil recovery rate ($L\ m^{-2}\ h^{-1}$)	Oil flux ($L\ m^{-2}\ h^{-1}\ bar^{-1}$)	Ref.
2022, Sep. Purif. Technol.	Pump-assisted	Toluene	-	16,663	6
2020, J. Membr. Sci.		Silicone oil	44	4,444	7
2019, Chem. Eng. J.		Diesel	-	18,000	8
2022, ACS Nano		Octane	-	2,993	9
2023, NPJ Clean Water		Hexane	294	294	10
2022, Nat. Commun.		Hexane	-	620	11
2022, Chem. Eng. J.		Soybean oil	27	13.5	12
2022, Chem. Eng. J.		Isooctane	1040	520	12
2021, J. Membr. Sci.		Hexane	1000	1,000	13
2022, Chem. Eng. Sci.		Heptane	-	7,146.7	14
2015, J. Mater. Chem. A		Toluene	-	41,880	15
2014, ACS Appl. Mater. Interfaces		Toluene	-	7,000	16
2015, J. Mater. Chem. A		Isooctane	-	22,590	17
2021, ACS Appl. Mater. Interfaces		Toluene	-	1,078	18
2024, J. Membr. Sci.	Filtration-type	Crude oil	-	1246	19
2023, J. Hazard. Mater.		Crude oil	-	779	20
2014, J. Mater. Chem. A		Hexane	-	5,000	21
2013, Adv. Mater.		Petroleum ether	-	10,000	22
2021, Sep. Purif. Technol.		Diesel	-	10,374	23
2021, Sep. Purif. Technol.		Toluene	-	23,794	23
2021, J. Membr. Sci.		Hexane	-	492.6	24
2021, J. Membr. Sci.		Soybean oil	-	82.1	24
2021, ACS Appl. Mater. Interfaces		Dichloromethane	-	21,799	25
2021, J. Membr. Sci.		Hexane	65	7,700	13
2019, ACS Nano	Siphon-assisted	Mineral oil	123.3	35,948	26
2023, Nano Energy		Mineral oil	105.8	28,561	2
2022, J. Mater. Chem. A		Mineral oil	318.8	81,000	27
Our work		**Mineral oil**	**620.2 (indoor)**	**136,982 (indoor)**	-
Our work		**Mineral oil**	**938.2 (outdoor)**	**207,218 (outdoor)**	-

References

(1) Wu, S.; Tian, S.; Jian, R.; Zhou, L.; Luo, T.; Xiong, G. Bio-Inspired Salt-Fouling Resistant Graphene Evaporators for Solar Desalination of Hypersaline Brines. *Desalination* **2023**, *546*, 116197. https://doi.org/10.1016/j.desal.2022.116197.

(2) Wu, S.; Jian, R.; Tian, S.; Zhou, L.; Luo, T.; Xiong, G. Simultaneous Solar-Driven Seawater Desalination and Continuous Oil Recovery. *Nano Energy* **2023**, *107*, 108160. https://doi.org/10.1016/j.nanoen.2022.108160.

(3) Tian, S.; Zhou, L.; Wu, S.; Jian, R.; Keewan, A.; Cui, S.; Xiong, G. Multifunctional Superelastic Graphene Aerogels Derived from Ambient-Dried Graphene Oxide/Camphene Emulsions. *Materials Letters* **2022**, *328*, 133128. https://doi.org/10.1016/j.matlet.2022.133128.

(4) Qiu, L.; Sun, Y.; Guo, Z. Designing Novel Superwetting Surfaces for High-Efficiency Oil–Water Separation: Design Principles, Opportunities, Trends and Challenges. *J. Mater. Chem. A* **2020**, *8* (33), 16831–16853. https://doi.org/10.1039/D0TA02997A.

(5) Kota, A. K.; Kwon, G.; Choi, W.; Mabry, J. M.; Tuteja, A. Hygro-Responsive Membranes for Effective Oil–Water Separation. *Nature Communications* **2012**, *3* (1), 1025. https://doi.org/10.1038/ncomms2027.

(6) Zhao, C.; Huang, H.; Li, Z.; Li, J.; Li, Y.; Xiang, D.; Wu, Y.; Chen, J.; Chen, X.; Qin, M. 3D Superhydrophobic/Superoleophilic Sponge with Hierarchical Porous Structure and Robust Stability for High-Efficiency and Continuous Separation of Oily Wastewater. *Separation and Purification Technology* **2022**, *299*, 121820. https://doi.org/10.1016/j.seppur.2022.121820.

(7) Zhao, L.; Li, R.; Xu, R.; Si, D.; Shang, Y.; Ye, H.; Zhang, Y.; Ye, H.; Xin, Q. Antifouling Slippery Liquid-Infused Membrane for Separation of Water-in-Oil Emulsions. *Journal of Membrane Science* **2020**, *611*, 118289. https://doi.org/10.1016/j.memsci.2020.118289.

(8) Yang, J.; Wang, H.; Tao, Z.; Liu, X.; Wang, Z.; Yue, R.; Cui, Z. 3D Superhydrophobic Sponge with a Novel Compression Strategy for Effective Water-in-Oil Emulsion Separation and Its Separation Mechanism. *Chemical Engineering Journal* **2019**, *359*, 149–158. https://doi.org/10.1016/j.cej.2018.11.125.

(9) Cheng, X.; Ye, Y.; Li, Z.; Chen, X.; Bai, Q.; Wang, K.; Zhang, Y.; Drioli, E.; Ma, J. Constructing Environmental-Friendly "Oil-Diode" Janus Membrane for Oil/Water Separation. *ACS Nano* **2022**, *16* (3), 4684–4692. https://doi.org/10.1021/acsnano.1c11388.

(10) Baig, N.; Abdulazeez, I.; Aljundi, I. H. Low-Pressure-Driven Special Wettable Graphene Oxide-Based Membrane for Efficient Separation of Water-in-Oil Emulsions. *npj Clean Water* **2023**, *6* (1), 40. https://doi.org/10.1038/s41545-023-00252-y.

(11) Yang, C.; Long, M.; Ding, C.; Zhang, R.; Zhang, S.; Yuan, J.; Zhi, K.; Yin, Z.; Zheng, Y.; Liu, Y.; Wu, H.; Jiang, Z. Antifouling Graphene Oxide Membranes for Oil-Water Separation via Hydrophobic Chain Engineering. *Nature Communications* **2022**, *13* (1), 7334. https://doi.org/10.1038/s41467-022-35105-8.

(12) Chen, X.; Dai, C.; Zhang, T.; Xu, P.; Ke, W.; Wu, J.; Qiu, M.; Fu, K.; Fan, Y. Efficient Construction of a Robust PTFE/Al2O3 Hydrophobic Membrane for Effective Oil Purification. *Chemical Engineering Journal* **2022**, *435*, 134972.

https://doi.org/10.1016/j.cej.2022.134972.
(13) Zhang, X.; Liu, C.; Yang, J.; Huang, X.-J.; Xu, Z.-K. Wettability Switchable Membranes for Separating Both Oil-in-Water and Water-in-Oil Emulsions. *Journal of Membrane Science* **2021**, *624*, 118976. https://doi.org/10.1016/j.memsci.2020.118976.
(14) Zhang, S.; Su, Q.; Yan, J.; Wu, Z.; Tang, L.; Xiao, W.; Wang, L.; Huang, X.; Gao, J. Flexible Nanofiber Composite Membrane with Photothermally Induced Switchable Wettability for Different Oil/Water Emulsions Separation. *Chemical Engineering Science* **2022**, *264*, 118175. https://doi.org/10.1016/j.ces.2022.118175.
(15) Gu, J.; Xiao, P.; Huang, Y.; Zhang, J.; Chen, T. Controlled Functionalization of Carbon Nanotubes as Superhydrophobic Material for Adjustable Oil/Water Separation. *J. Mater. Chem. A* **2015**, *3* (8), 4124–4128. https://doi.org/10.1039/C4TA07173E.
(16) Gu, J.; Xiao, P.; Chen, J.; Zhang, J.; Huang, Y.; Chen, T. Janus Polymer/Carbon Nanotube Hybrid Membranes for Oil/Water Separation. *ACS Appl. Mater. Interfaces* **2014**, *6* (18), 16204–16209. https://doi.org/10.1021/am504326m.
(17) Hu, L.; Gao, S.; Zhu, Y.; Zhang, F.; Jiang, L.; Jin, J. An Ultrathin Bilayer Membrane with Asymmetric Wettability for Pressure Responsive Oil/Water Emulsion Separation. *J. Mater. Chem. A* **2015**, *3* (46), 23477–23482. https://doi.org/10.1039/C5TA03975D.
(18) Wang, J.; He, B.; Ding, Y.; Li, T.; Zhang, W.; Zhang, Y.; Liu, F.; Tang, C. Y. Beyond Superwetting Surfaces: Dual-Scale Hyperporous Membrane with Rational Wettability for "Nonfouling" Emulsion Separation via Coalescence Demulsification. *ACS Appl. Mater. Interfaces* **2021**, *13* (3), 4731–4739. https://doi.org/10.1021/acsami.0c19561.
(19) Xiang, B.; Gong, J.; Sun, Y.; Yan, W.; Jin, R.; Li, J. High Permeability PEG/MXene@MOF Membrane with Stable Interlayer Spacing and Efficient Fouling Resistance for Continuous Oily Wastewater Purification. *Journal of Membrane Science* **2024**, *691*, 122247. https://doi.org/10.1016/j.memsci.2023.122247.
(20) Yu, J.; Cao, C.; Pan, Y. A Solar-Driven Degradation-Evaporation Strategy for Membrane Self-Cleaning in the Efficient Separation of Viscous Crude Oil/Water Emulsions. *Journal of Hazardous Materials* **2023**, *457*, 131826. https://doi.org/10.1016/j.jhazmat.2023.131826.
(21) Gu, J.; Xiao, P.; Chen, J.; Liu, F.; Huang, Y.; Li, G.; Zhang, J.; Chen, T. Robust Preparation of Superhydrophobic Polymer/Carbon Nanotube Hybrid Membranes for Highly Effective Removal of Oils and Separation of Water-in-Oil Emulsions. *J. Mater. Chem. A* **2014**, *2* (37), 15268–15272. https://doi.org/10.1039/C4TA01603C.
(22) Zhang, W.; Shi, Z.; Zhang, F.; Liu, X.; Jin, J.; Jiang, L. Superhydrophobic and Superoleophilic PVDF Membranes for Effective Separation of Water-in-Oil Emulsions with High Flux. *Advanced Materials* **2013**, *25* (14), 2071–2076. https://doi.org/10.1002/adma.201204520.
(23) Zhang, T.; Xiao, C.; Zhao, J.; Liu, X.; Ji, D.; Zhang, H. One-Step Facile Fabrication of PVDF/Graphene Composite Nanofibrous Membrane with Enhanced Oil Affinity for Highly Efficient Gravity-Driven Emulsified Oil/Water Separation and Selective Oil Absorption. *Separation and Purification Technology* **2021**, *254*, 117576. https://doi.org/10.1016/j.seppur.2020.117576.
(24) Xie, A.; Cui, J.; Liu, Y.; Xue, C.; Wang, Y.; Dai, J. Preparation of Janus Membrane Based on Biomimetic Polydopamine Interface Regulation and Superhydrophobic

Attapulgite Spraying for On-Demand Oil-Water Emulsion Separation. *Journal of Membrane Science* **2021**, *627*, 119242. https://doi.org/10.1016/j.memsci.2021.119242.

(25) Ding, Y.; Xu, S.; Zhang, H.; Zhang, J.; Qiu, Z.; Chen, H.; Wang, J.; Zheng, J.; Wu, J. One-Step Fabrication of a Micro/Nanosphere-Coordinated Dual Stimulus-Responsive Nanofibrous Membrane for Intelligent Antifouling and Ultrahigh Permeability of Viscous Water-in-Oil Emulsions. *ACS Appl. Mater. Interfaces* **2021**, *13* (23), 27635–27644. https://doi.org/10.1021/acsami.1c05896.

(26) Wu, S.; Yang, H.; Xiong, G.; Tian, Y.; Gong, B.; Luo, T.; Fisher, T. S.; Yan, J.; Cen, K.; Bo, Z.; Ostrikov, K. K. Spill-SOS: Self-Pumping Siphon-Capillary Oil Recovery. *ACS Nano* **2019**, *13* (11), 13027–13036. https://doi.org/10.1021/acsnano.9b05703.

(27) Wu, S.; Tian, S.; Jian, R.; Wu, T.-N.; Milazzo, T. D.; Luo, T.; Xiong, G. Graphene Petal Foams with Hierarchical Micro- and Nano-Channels for Ultrafast Spontaneous and Continuous Oil Recovery. *J. Mater. Chem. A* **2022**, *10* (21), 11651–11658. https://doi.org/10.1039/D2TA00019A.